Squeezing Oil into Water under Pressure: Inverting the Hydrophobic Effect

Squeezing Oil into Water under Pressure: Inverting the Hydrophobic Effect

Ciprian G. Pruteanu,[*,†] Victor Naden Robinson,[*,‡] Narjes Ansari,[‡] Ali Hassanali,[‡] Sandro Scandolo,[‡] and John S. Loveday[¶]

†*Department of Physics and Astronomy, University College London, Gower Street, London WC1E 6BT, United Kingdom*

‡*The "Abdus Salam" International Centre for Theoretical Physics, I-34151 Trieste, Italy*

¶*SUPA, School of Physics and Astronomy and Centre for Science at Extreme Conditions, The University of Edinburgh, Edinburgh EH9 3JZ, United Kingdom*

E-mail: cip.pruteanu@ucl.ac.uk; victornadenrobinson@gmail.com

Abstract

The molecular structure of dense homogeneous fluid water-methane mixtures has been determined for the first time using high-pressure neutron-scattering techniques at 1.7 and 2.2 GPa. A mixed state with a fully H-bonded water network is revealed. The hydration shell of the methane molecules is however revealed to be pressure dependent with an increase in the water co-ordination between 1.7 and 2.2 GPa. In parallel, *ab initio* molecular dynamics simulations have been performed to provide insight into the microscopic mechanisms associated with the phenomenon of mixing. These calculations reproduce the observed phase change from phase separation to mixing with increasing pressure. The calculations also reproduce the experimentally observed structural properties. Unexpectedly, the simulations show mixing is accompanied by a subtle enhancement of the polarization of methane. Our results highlight the key role played by fine electronic effects on miscibility and the need to re-adjust our fundamental understanding of hydrophobicity to account for these.

Graphical TOC Entry

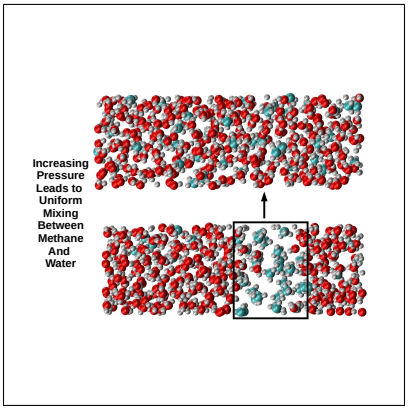

Keywords

water,methane,neutron scattering,simulation,high pressure

Introduction

Common experience tells us that oil and water are not miscible.[1] The separation of oil and water is the cornerstone of the hydrophobic effect.[2] Methane is the shortest hydrocarbon and is insoluble in water at ambient conditions[1] (0.006 mole % solubility at 100°C and 10 MPa). In this regard, the thermodynamics associated with the interaction of methane with water forms a classic textbook problem. Hydrophobic interactions are a fundamental and ubiquitous phenomenon since they underpin many crucial life-enabling processes such as protein folding[3] and cell membrane formation.[4] Hydrophobicity also plays a central role in chemical engineering problems, for example, in the food industry.[5]

The evolution of hydrophobic interactions under different thermodynamic conditions is relevant to a wide range of science ranging from Earth and planetary sciences to biology and is consequently a longstanding active field of research.[6–8] Methane-water mixtures are present at the bottom of oceans, where compression leads to the formation of solid methane hydrates,[9] they are also major constituents of the middle layers of the ice giants Neptune and Uranus,[10] and icy satellites like Titan and Triton.[11] Combinations of water, ammonia, and methane are predicted to be widely present in recently observed exoplanets, which have been most commonly of Neptune-like proportions,[12–14] and are likely to exist as either liquids or solids.[15–18] A microscopic understanding of how extreme pressures modulate the solubility of methane-water mixtures is thus critical in order to develop realistic models of the interior of planets.[19]

Hydrophobic interactions are central in the underlying architecture of biological machinery. Over half a century ago, several different experiments showed the effects of pressure on biochemical processes such as protein folding and later on in chemical reactions.[6] It is now well established for example, that the phase diagram of proteins is very sensitive to pressure.[20–22] Specifically, single-chained proteins are known to denature at pressures of about

100 MPa. Protein unfolding and denaturation have been generally linked to a pressure-induced weakening of hydrophobic interactions,[23] but the molecular mechanisms associated with these phenomena remain poorly understood.

Methane generally shows a sub-linear tendency of solubility increase with pressure in the range up to ~ 1 GPa so that the maximum solubility remains significantly below 1 mol %.[24,25] However, it was shown recently that starting at 1.3 GPa, the solubility of methane in water begins to increase dramatically and eventually saturates at a maximum of 44(3) mol % at 1.9 GPa and 373 K.[26] The microscopic origin of the increased solubility observed in these experiments is not clear. Chandler proposed that enhanced pressures would result in a disruption of the hydrogen bond network leading to increased solubility.[27] However, the extent to which hydrophobic molecules disrupt the hydrogen bond network has been challenged by a combination of both simulations and experiment which find a fully H-bonded network is maintained to high pressure.[28,29] Moreover attempts to obtain a microscopic understanding failed because standard intermolecular potentials, with sufficiently large unit cells, do not give a mixed state.[30]

Here we report combined experimental and theoretical studies which reveal how the hydrophobic effect is inverted under pressure in methane-water mixtures. Our neutron scattering experiments reveal the local structure of the mixed fluid in the pressure range 1.7 GPa to 2.2 GPa. *Ab-initio* molecular-dynamics simulations of the methane-water mixtures confirm the experimental observables and show an enhancement of interactions between the methane and water molecules due to a subtle increase in the methane dipole moment. These effects were not captured by standard classical potentials which failed at reproducing pressure-induced enhanced solubility.[30] The measured and calculated structure and topology of water shows that methane mixing does not involve a significant change in the hydrogen bond network as it adapts to the presence of methane.

Methods

Experimental details

Both measurements of the fluid structure were performed on the PEARL beamline at the ISIS Neutron Spallation Source, Rutherford-Appleton Laboratory, UK. Samples of fully occupied methane hydrate I (MH-I, 5.75:1 water:methane content) were cryo-loaded in a Paris-Edinburgh high volume press.[31] A liquid nitrogen-cooled TiZr gasket was filled with the sample, and then placed in pre-cooled anvils and a 5 tonne sealing-load applied. The samples were compressed to the desired pressures and warmed to 413 K (where no crystalline content could be detected). Data were collected for 48 hours for each run, followed by a 24 hour collection of background and 24 hour collection of vanadium needed for normalization. Data analysis was performed using the EPSR (empirical potential software refinement)[32] package having 1000 molecules simulation boxes with the same composition as the samples. The density of the fluid mixture was estimated using a linear combination of the known equations of state for fluid water[33] and methane.[34] After equilibriation and fitting, the individual pair distribution functions were sampled over 10000 accumulations. For the initial setup of the simulation box the molecules were defined using the TIP3P parameters for water (for OH bond lengths and dihedral angle) and the OPLS-AA parameters for methane as described by Kaminski et al.[35]

Computational details

The AIMD simulations were performed with the CP2K package using Quickstep.[36] The wavefunction was expanded using both a TZVP Gaussian basis set and a plane wave representation using a cutoff of 300 Ry. The Becke, Lee, Yang, and Parr (BLYP) exchange-correlation,[37,38] was used together with the Grimme D3 empirical corrections for the Van der

Waals interactions.[39] Norm-conserving Goedecker-Teter-Hutter (GTH) pseudopotentials[40] were used for treating the core electrons. The AIMD simulations were integrated with a time step of 0.5 fs within the NVT ensemble using the canonical sampling through velocity rescaling (CSVR) thermostat,[41] thermostatting the system at 413 K. Mixture boxes with 300 molecules had sizes at low pressure of 45.0×15.0×15.0 Å corresponding to a density of 870 kg/cm^3 and a pressure of 0.2 GPa, where high pressure sizes refer to pressures of 1.2 and 2.3 GPa (see SI). Initial conditions for mixed systems were created from the experimental s(q) fitting and then expanded into a 311 orthorhombic box. Demixed systems were created from classical potential simulations, which favour this demixing. To reveal phase whether phase separation or mixing occurred long simulations of up to 250 ps were performed.

Results and discussion

Figure 1(a) shows the pair (or radial)-distribution functions (PDFs) obtained from neutron scattering data. The total-scattering patterns (see SI) obtained showed few, clearly localized broad peaks with no sign of heterogeneity, ruling out the possibility of an emulsion. Molecular-level homogeneous mixing is supported by the further analysis: high quality fits did not require methane or water clustering or cluster-size re-scaling as commonly encountered in emulsions.[42] The extracted PDFs are all smooth and monotonically decaying, as expected for simple fluids.[43] By contrast, more complex systems that present bonding and local ordering or clustering tend to yield significantly more feature-rich distribution functions, such as SiO_2 melts.[44] The total scattering data showed an increase in CH_4-H_2O coordination with increasing pressure (Figure 1(b)), and a simultaneous decrease in CH_4-CH_4 coordination seen in Figure 3. This is accompanied by very little change in the structure of water, which tends to maintain its normal coordination and H-bonding structure (Figure 1(c)). Conversely, the decreased methane-methane coordination is accompanied by increased water co-ordination (see Figure 1(b) and 1(d)). Both the C-O and and C-H_{H_2O} partial g(r)'s

show clear increases in the height of the first peak at 2.2 GPa. Integration of these curves out to the first minimum shows an increase in water co-ordination of ∼0.6 molecules. Furthermore, the first co-ordination shell sharpens so that the co-ordination out to 4.38 Å increases by almost 2 water molecules.

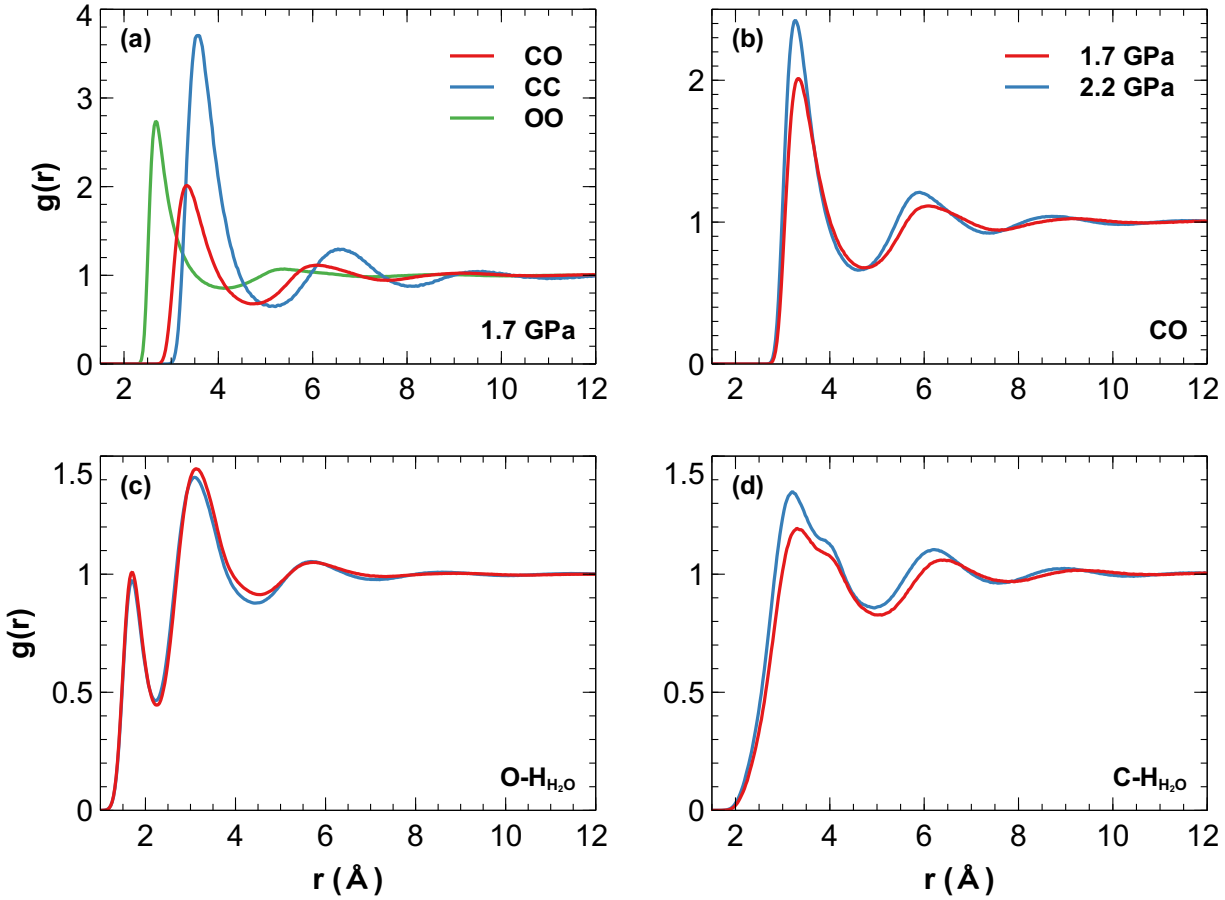

Figure 1: PDFs from EPSR; (a) Water-water, methane-methane and methane-water for the sample at 1.7 GPa; (b) Methane-water (C-O) for both 1.7 and 2.2 GPa; (c) O-H $_{H_2O}$, for 1.7 and 2.2 GPa; (d) C-H$_{H_2O}$ for both 1.7 and 2.2 GPa. Changes in miscibility with pressure (such as C-O) can be noticed, meanwhile the O-O remains largely unaffected. i.e. the water-methane space is still much more compressible, while O-O is at smaller separation than pure water at the same pressure.

Using EPSR's built-in capabilities to calculate spatial correlation functions, especially spatial distribution functions and dipole moment orientations, we found that water's dipole moment points away from the methane molecules (see SI), similar to the situation reported

at lower pressure by Koh et al.[45] during hydrate formation. Moreover, Buchanan et al.[46] found that at 180 bars and 18°C the presence of dissolved methane in water causes a compression of the second shell of water, similar to but smaller than the effect of high pressure on pure water. We notice a significantly more collapsed second shell, due to the combination of both higher pressure and over an order of magnitude more methane being present in the mixture (14.8 mole % in our case, 0.3 mole % in Buchanan's). The authors also noted there are 16±1 water molecules coordinating a given methane molecule, whereas we find slightly below and above 13 for 1.7 and 2.2 GPa respectively. The number of neighbouring water molecules is expected to decrease in a solution having a significantly higher methane content despite also being at much higher pressures (which naturally tends to increase the number of neighbours at a given fixed distance).

In order to provide more insights into the molecular origins of the pressure induced mixing, we performed a series of *ab initio* molecular dynamics simulations. *Ab initio* simulations, while more accurate than classical simulations since they explicitly include the electronic degrees of freedom, are computationally more intensive and thus require prudent choice of system sizes and simulation times. A series of different initial conditions were constructed in order to study the mixing/de-mixing at 0.2, 1.2, and 2.3 GPa. Specifically, we began with two limiting cases: a mixed configuration obtained from the EPSR refinement at 1.7 GPa and a slab-like geometry corresponding to an initial de-mixed state (see Methods).

Figure 2 highlights some of the key initial findings of our simulations that confirm the experimental observations. Initial and final snapshots obtained from a 130 ps trajectory at 0.2 GPa illustrate clearly that the system irreversibly de-mixes to form a slab-like geometry. This is also quantified in the time-dependent PDFs shown at the top of Figure 2 reporting an increase in the methane coordination and a decrease in the solvent exposure of the methane molecules over time.

This phenomenon is distinct from the interfacial mixing previously observed at ambient pressure[47–49] and shows that our simulations are able to mix and demix the system on *ab initio* time scales.

Initial and final configurations that were obtained from the simulations at 1.2 GPa starting from a slab-geometry are shown in the SI. Interestingly, over a timescale of 30-50 ps, we observe water molecules penetrating into the slab which results in methane molecules breaking away from the cluster. The timescales associated with the mixing are very slow and the simulations (200 ps at 1.2 GPa) are not long enough to capture the kinetics associated with this process required to generate fully mixed configurations. After 200 ps at 1.2 and 250 ps at 2.3 GPa respectively the mixing process is evident, yet slower than the demixing at 0.2 GPa.

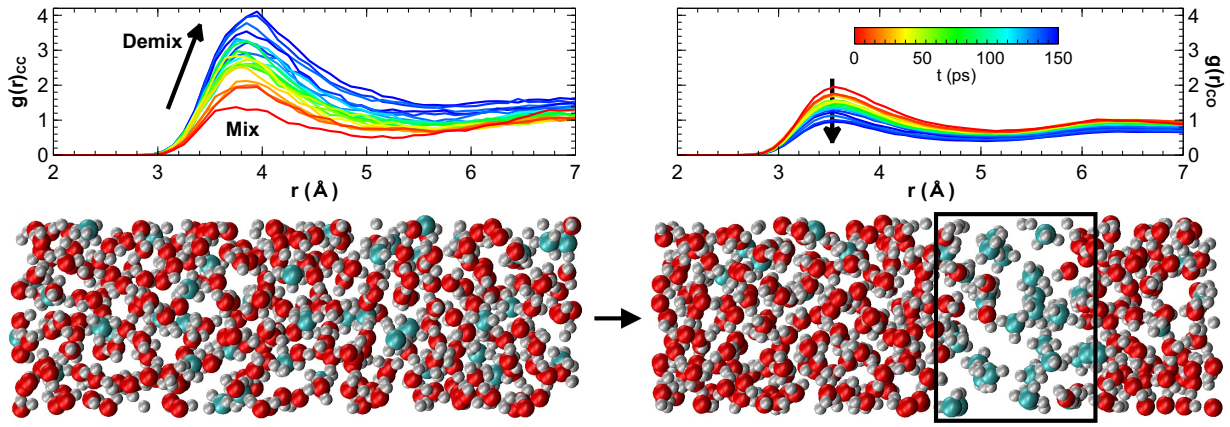

Figure 2: (Above) PDF's showing demixing at 0.2 GPa as CC grows and CO reduces over time, forming the slab seen below. (Below) Initial and final (150 ps) snapshots at 0.2 GPa where the mixed system begins to phase separate into a slab.

In order to assess the quality of the mixed methane-water simulations, we show in Figure 3 the pair distribution functions and associated coordination numbers for the mixture at 1.2 GPa. The differences observed between the experimental and simulation PDFs are largely due to the different pressures of 1.2 and 1.7 GPa and are reflected more in the $g(r)_{CC}$.

These differences can also be attributed to simulation sensitivity to equilibration, differences in mixing concentration (14% vs. 14.8%), the possibility of having small emulsions in the sample, the EPSR CH bond length and OPLSS-AA methane potential, and ab initio lacking a perfect physical description of interactions. Better agreement could be made if the initial conditions were closer to the g(r) distributions that EPSR converged upon (see SI). The fact that the pure CH_4 $g(r)_{CC}$ is not hugely different from that of the mixture implies that CH_4-CH_4 distances are similar but with much lower CC c_n in the mixture.

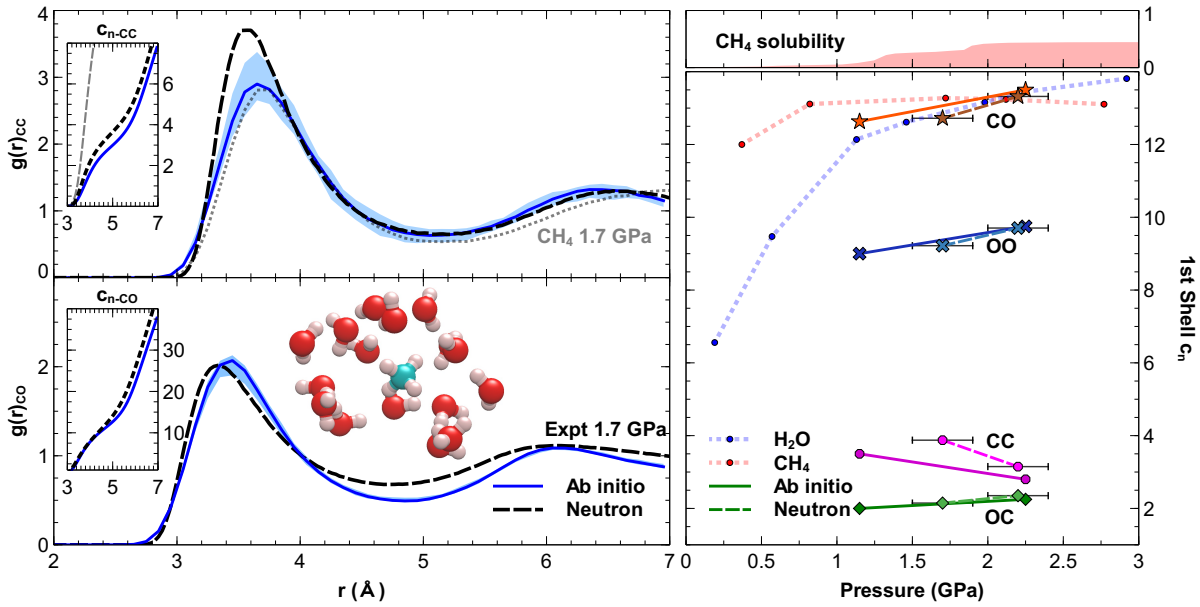

Figure 3: (Left) PDFs and inset running coordination numbers (c_n) from AIMD (blue line, 1.2 GPa) compared to experimental (dashed black line, 1.7 GPa) and those of pure phases from AIMD (dotted grey lines). A fluctuation confidence window is included by a blue shaded region. (Right) All c_n's from integrating up to the first minima of PDFs for neutron data (dashed lines) and ab initio (solid lines). Top panel shows the maximal solubility as a function of pressure as reported by Pruteanu et al.[26] Pure systems are included for reference, and symbols match the type of atom pair. While the data points are few, there is strong overlap between experiment and simulation, which are likely probing the very same liquid.

The pressure evolution of the coordination numbers, and a comparison to the pure phases of water and methane respectively, are shown in Figure 3. Consistent with the PDFs reported earlier, there is a clear increase with pressure in the number of oxygen atoms within the first

shell (c_n) of a given methane molecule , accompanied by a similar decrease in the number of neighboring methane molecules. The structure of solvated water molecules (water molecules neighbouring other water molecules) also increases but remains lower than that of pure water due to the excluded-volume effect owing to the presence of methane. Computed spatial distribution functions from AIMD reinforce this (see SI), being in good agreement with those calculated by EPSR. One can also notice that around 2 GPa, the number of water molecules within the first shell of a methane one in the mixture equals that of all neighbouring molecules in the pure phase. The effect of solvating methane we observe here is akin to previous simulations by Hummer and co-workers which examined the potential of mean force using classical potentials between two methane molecules in water as a function of pressure.[23] An increase in pressure appears to destabilize the contact minimum between two methane molecules and stabilize the solvent-separated state.

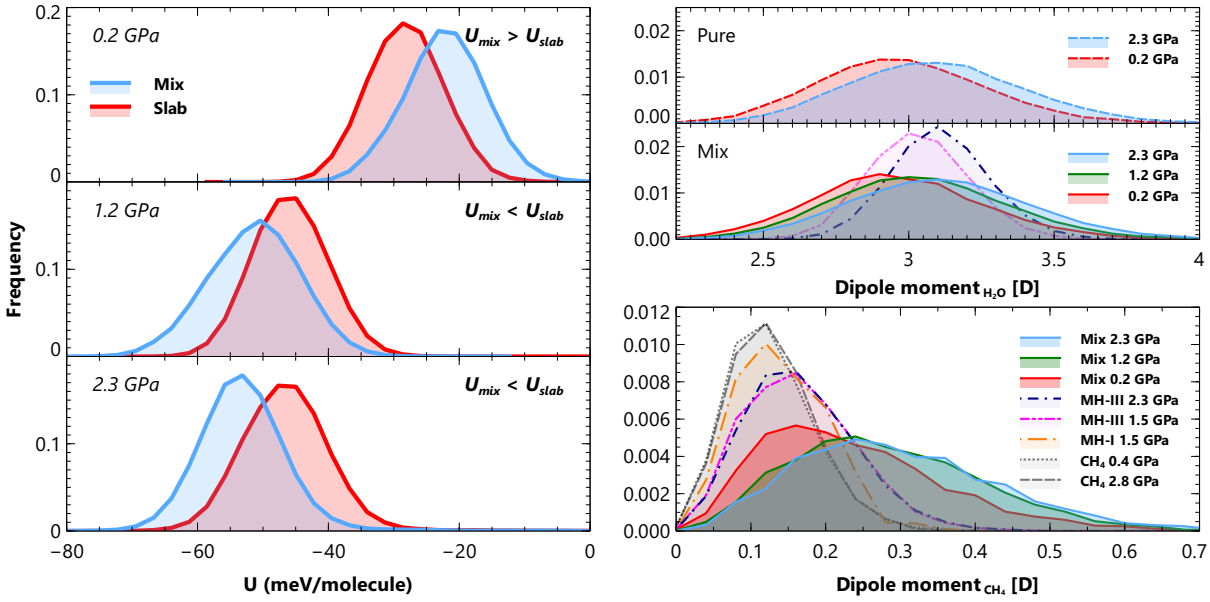

Figure 4: (Left) The distribution of internal energy, U, plotted for the different systems in mixed or demixed states. With increasing pressure, the internal energy shows that the mixed system becomes more stable. (Right) Shows the distribution of dipole moments for methane and water molecules. Increasing pressure shows that the water dipole does not change significantly, though the mixed system has a greater dipole moment due to the shorter O-O distance for the same pressure as the pure system. For methane, the mixed system causes a subtle enhancement of dipole moment due to the presence of dense water molecules, far more so than in the solid hydrates (I,III) shown at 300 K.

The combined experimental and simulation results up to this point, show that an increase in pressure leads to suppression of the hydrophobic effect. In order to understand better the microscopic origin of this phenomenon, we next examine the thermodynamic signatures associated with mixing. It is beyond the scope of the current calculations to compute the free energies of mixing/demixing. However, mixing is always entropically favored and in this particular case the entropy of mixing is found to be close to that of an ideal random mixture, both at 1.2 and 2.3 GPa (calculated using the same method as in Pruteanu et al.,[30] see SI). We will therefore focus on the evolution of the internal energy on mixing. In the left panel of Figure 4 the internal energies of mixed and unmixed simulations are shown at 0.2, 1.2, and 2.3 GPa. At 0.2 GPa U was calculated before the system starts to phase separate. Interestingly, at both 1.2 and 2.3 GPa, the mixed simulation of methane and water is lower in energy, by about 10 meV/molecule. At 0.2 GPa, where the methane molecules cluster together, the slab conditions are lower in energy compared to the mixed state. The stabilization of the methane-water interactions at high pressure thus correspond to about 12 meV/molecule, roughly 5% of the cohesive energy for a water molecule dimer. This suggests internal energy is strongly influencing the mixing driving force and importantly turns over from unfavoring to favoring mixing with pressure.

Earlier, we stated that previously performed classical molecular dynamics simulations failed, even qualitatively, to reproduce the trends observed in the experiments.[30] One possible origin of this failure is that the increase in pressure leads to subtle changes in the electronic properties of both methane and water which cannot be captured by the TIP3P, TIP4P, SPCE and OPLS-AA potentials, for example in the molecular polarization. Previous theoretical studies have also suggested the importance of methane polarization in methane hydrates.[50] In order to assess the role of polarization in our simulations, we examined the molecular dipole distributions of pure, mixed and slab-like systems. The dipole moment was calculated using maximally localized Wannier functions (WCs).[51] The total molecular dipole

is given by $\boldsymbol{D}_{tot} = -\sum_i 2e\boldsymbol{r}_i + \sum_I Q_I \boldsymbol{R}_I$ where $\boldsymbol{R}_I$ is the position of the ion center , $\boldsymbol{r}_i$ is the position of the Wannier centre, and Q_I is the ionic charge.

The dipole moments are shown for water and methane molecules in the top and bottom panels respectively. Overall, the increase in pressure results in an increase in the dipole moment of water by 0.13 D at 2.3 GPa: the dipole moments in pure water at ambient and 2.3 GPa are 2.97±0.08 D and 3.10±0.09 D respectively (the uncertainties are estimated from the variances.). For methane in the mixture, the change is quite remarkable . At just 1.2 GPa, the dipole moment increases to roughly 0.3 D and remains almost the same at 2.3 GPa. For reference, methane molecules in the pure phase are non-polar and characterized by a very small and pressure-independent dipole moment and fluctuations (calculated here as 0.1 D). For the 0.2 GPa mixed system the snapshots were taken from the first part of the simulation before the system has demixed. The increased dipole moments of the methane molecules we observe are consistent with previous *ab initio* simulations that were performed at much higher temperatures and pressures,[17] yet here they occur at much lower pressures and temperatures.

It is well appreciated the inclusion of dispersion interactions is critical for reproducing both structural and dynamical properties of aqueous systems with DFT.[52] Although we have included dispersion interactions using the empirical Grimme correction, we wanted to assess the sensitivity of some of our results to the choice of using more accurate non-local dispersion functionals. For this reason, we performed simulations using both DRSLL[53] and rVV10[54] functionals for the methane-water mixtures at 1.2 GPa and for 20 ps. The dipole moment distributions are consistently reproduced by all of these functionals.

Methane in the gas phase would, due to symmetry, have no permanent dipole. The non-zero methane dipole seen in our simulations arises from fluctuation induced symmetry

breaking. This is a feature that appears to be enhanced at high pressure relative to ambient conditions. At high pressure, the presence of a large fluctuating dipole has already been observed in previous first principles simulations.[17] We find that the magnitude of the fluctuating dipole of methane is not short lived (see SI Figure 34) which shows the dipole moment for a single methane molecule as a function of time. The magnitude of the dipole fluctuates between 0.05 and 0.7 D on the time scales of picoseconds, while the average of the magnitude of the dipole moments of all the CH_4 molecules is roughly constant at 0.3 D. As expected, the average of each component of the dipole vector of methane is zero, however the fluctuations away from zero are roughly twice as large in the mixture at 1.2 GPa compared with the pure methane system. It is these strong fluctuations of the vector from zero that boost the magnitude of the dipole moment for methane.

The enhanced dipole moment of methane under pressure does not imply that it has a permanent dipole moment, but a finite dipole arises from enhanced fluctuations of the three components of the dipole vector. In SI Figure 32, we observe that all three components of the dipole are well approximated by Gaussian distributions with the same spread implying no symmetry breaking. However, under pressure the enhanced fluctuations of all three components leads to an increase of methane's dipole moment, consistent with previous studies.[17]

The increase in interactions between the methane molecules and water has a rather subtle effect on the water hydrogen-bond network. We first examined the number of hydrogen bonds formed between water molecules in both pure water up to 3 GPa and in the methane-water mixtures which is shown in Figure 5. Hydrogen bonds were determined by using a geometrical criterion developed by Luzar and Chandler.[55] Interestingly, we observe that the water hydrogen-bond network retains its integrity in the mixture. We find that the mixed system contains 97% of H-bonds found in the pure water system at both 1.2 and 2.3 GPa. Although there are slightly fewer hydrogen bonds, they tend to be slightly stronger than in

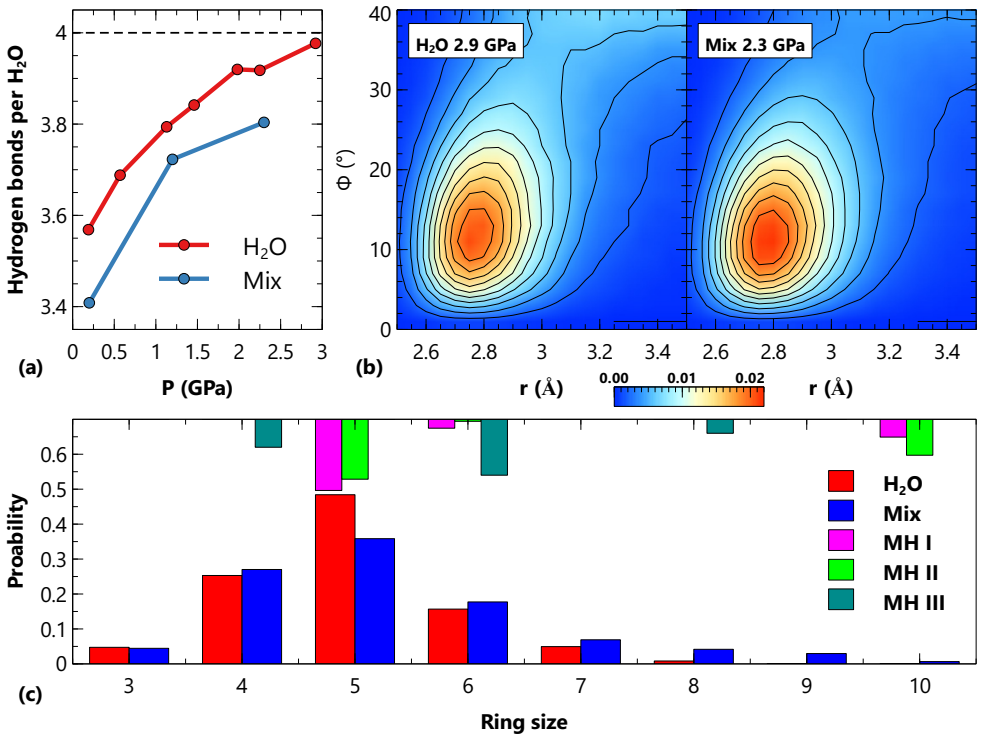

Figure 5: (Top-left) Water hydrogen bonds (cutoff at 3.5 Å and 35°) per water molecule and (top-right) 2D probability distribution of closest hydrogen bonds for pure water at 2.9 GPa and the mix at 2.3 GPa. (Bottom) Ring statistics at 1.2 GPa (mixture) and 1.1 GPa (water) with ticks plotted at the top representing closed rings found in methane hydrate (MH) phases I-III.

pure water: the bond angle and bond distance distributions are slightly smaller, with greater weight at smaller angles and distances, in the mixture (see SI). Our results are thus fully consistent with some recent experiments and simulations by Gradolnik et al.[29] that found a tendency for pure hydrophobic solutes to strengthen and enhance hydrogen-bonding rather than weaken it. It is likely that increased methane content (> 14 %) reduces the local dipole field of the water molecules, and this may limit the solubility of methane to the observed value of 44 % at 3 GPa.

In order to examine the structural effects of methane mixing at high pressure on the topology of the hydrogen bond network, we examined the distribution of closed rings made up of hydrogen bonded water molecules in the different systems. Ring distributions have

been in used in several previous studies to provide insight into the changes on the hydrogen bond network of water in the presence of solutes.[56–59] The ring statistics are shown in Figure 5(c) for three different systems: the mixed methane-water system, the de-mixed slab system, and pure water at 1.5 GPa. We observe that all the three systems are dominated by the presence of 5-membered rings. However, the number of 5-membered rings is highest for the pure water system and lowest for the methane mixture. Furthermore, the presence of water molecules interspersed by methane also results in an increase in the number larger rings as seen in the fatter tail of rings with 6 members or greater .

The presence of 4/5/6/8-membered rings has also been observed in low-pressure methane clathrates,[60,61] indicated in Figure 5. The mixture exhibits a greater number of rings, with a greater difference for 6 membered, consistent with MH-III (stable above 1.9 GPa), implying a similar clathrate-like structure in the mixed liquid but with greater flexibility for defects in the ring networks. Comparing liquid dipoles with MH-III, the mixture has greater fluctuations in both water and methane molecules. The methane dipole in the in the mixed liquid is stronger than in MH-III, partly due to the difference in methane content (0.14 vs 0.33), and due to the geometry restrictions of MH-III where methane molecules exist as pairs. However, methane dipoles in MH-I at 1.5 GPa reveal a distribution closer to that of pure methane, even though the MH-I methane content is 14 % as in the mixed liquid. In the solid hydrates, increasing pressure shows a tendency to increase the methane dipole moment, but we find this effect to be much stronger in the liquid.

Conclusions

The combined experimental and ab-initio modelling studies have revealed the structure of the pressure-mixed methane-water fluid. It has a fully hydrogen-bonded water network without significant broken hydrogen bonds, and increasing water to methane co-ordination with

increasing pressure and a reduction in width of the hydration shell. The modelling provides insight into what is changing at the onset of mixing. At a macroscopic level, mixing appears to be driven by a change with pressure in the enthalpy of mixing rather than a change in the entropy of mixing. Mixing is also accompanied by a change in the ring connectivity of the water network with a trend to larger rings than pure water.

Our results begin to understand the importance of electronic polarization on hydrophobic effects in soft-matter systems. Protein-water interactions, for example, will clearly be affected by subtle changes in the polarizability particularly under pressure and play an important role in tuning the phase diagram of protein stability. This opens up interesting challenges for the development of empirical forcefields for biological systems under extreme pressures.

Acknowledgement

This work was supported by the Engineering and Physical Sciences Research Council (EPSRC) through a Centre for Doctoral Training studentship and a Doctoral Prize Fellowship for C.G.P. The authors would like to thank ISIS Neutron Spallation Source, UK for the award of beamtimes (RB1820413 and RB1700058) and Dr. Craig Bull for assistance during the experiments; UCL Research Computing Services for CPU time on Grace; and CINECA for computing resources on Marconi.

Supporting Information Available: Simulation snapshots; Polarization and Wannier centres; Methane hydrate dipoles; Vibrational density of states; Table of simulation details; Pressure temperature phase diagram; Equation of state and pressure determination; Structure factors; Angular distribution functions; Entropy of mixing; Orientation dynamics; Methane hydrate Pair Distribution Functions; Fluid Mixture Pair Distribution Functions;

Spatial Density Functions and Dipole Moment Orientations; Dispersion, XC, and dipoles.

References

(1) Atkins, P.; De Paula, J.; Keeler, J. *Atkins' Physical Chemistry*; Oxford University Press, 2018.

(2) Chandler, D. Hydrophobicity: Two Faces of Water. *Nature* **2002**, *417*, 491.

(3) Zhou, R.; Huang, X.; Margulis, C. J.; Berne, B. J. Hydrophobic Collapse in Multidomain Protein Folding. *Science* **2004**, *305*, 1605–1609.

(4) Tanford, C. The Hydrophobic Effect and the Organization of Living Matter. *Science* **1978**, *200*, 1012–1018.

(5) Di Bonaventura, G.; Piccolomini, R.; Paludi, D.; D'orio, V.; Vergara, A.; Conter, M.; Ianieri, A. Influence of Temperature on Biofilm Formation by Listeria Monocytogenes on Various Food-contact Surfaces: Relationship with Motility and Cell Surface Hydrophobicity. *J. Appl. Microbiol.* **2008**, *104*, 1552–1561.

(6) Daniel, I.; Oger, P.; Winter, R. Origins of Life and Biochemistry Under High-Pressure Conditions. *Chem. Soc. Rev.* **2006**, *35*, 858–875.

(7) Ancilotto, F.; Chiarotti, G. L.; Scandolo, S.; Tosatti, E. Dissociation of Methane into Hydrocarbons at Extreme (Planetary) Pressure and Temperature. *Science* **1997**, *275*, 1288–1290.

(8) Schaack, S.; Ranieri, U.; Depondt, P.; Gaal, R.; Kuhs, W. F.; Gillet, P.; Finocchi, F.; Bove, L. E. Observation of Methane Filled Hexagonal Ice Stable up to 150 GPa. *Proc. Natl. Acad. Sci.* **2019**, *116*, 16204–16209.

(9) Hoffmann, R. Old Gas New Gas. *Am. Sci.* **2006**, *94*, 16–18.

(10) Bergstralh, J. T.; Miner, E. D.; Matthews, M. S. *Uranus*; University of Arizona Press, 1991.

(11) Grasset, O.; Sotin, C.; Deschamps, F. On the Internal Structure and Dynamics of Titan. *Planet. Space Sci.* **2000**, *48*, 617–636.

(12) Hubbard, W. B.; MacFarlane, J. J. Structure and Evolution of Uranus and Neptune. *J. Geophys. Res.* **1980**, *85*, 225–234.

(13) Rauer, H.; Catala, C.; Aerts, C.; Appourchaux, T.; Benz, W.; Brandeker, A.; Christensen-Dalsgaard, J.; Deleuil, M.; Gizon, L.; Goupil, M. J. et al. *The PLATO 2.0 mission*; 2014; Vol. 38; pp 249–330.

(14) Noack, L.; Snellen, I.; Rauer, H. Water in Extrasolar Planets and Implications for Habitability. *Space Sci. Revs.* **2017**, 877–898.

(15) Robinson, V. N.; Wang, Y.; Ma, Y.; Hermann, A. Stabilization of Ammonia-rich Hydrate Inside Icy Planets. *Proc. Natl. Acad. Sci.* **2017**, *114*, 9003–9008.

(16) Naden Robinson, V.; Marqués, M.; Wang, Y.; Ma, Y.; Hermann, A. Novel Phases in Ammonia-Water Mixtures under Pressure. *J. Chem. Phys.* **2018**, *149*, 234501.

(17) Lee, M.-S.; Scandolo, S. Mixtures of Planetary Ices at Extreme Conditions. *Nat. Commun.* **2011**, *2*, 185.

(18) Bethkenhagen, M.; Cebulla, D.; Redmer, R.; Hamel, S. Superionic Phases of the 1: 1 Water–Ammonia Mixture. *J. Phys. Chem. A* **2015**, *119*, 10582–10588.

(19) Marley, M. S.; Fortney, J. J. *Encyclopedia of the Solar System*; Elsevier, 2014; pp 743–758.

(20) Doster, W.; Friedrich, J. *Protein Folding Handbook*; John Wiley & Sons, Ltd, 2008; Chapter 5, pp 99–126.

(21) Smeller, L. Pressure–Temperature Phase Diagrams of Biomolecules. *Biochim. Biophys. Act.* **2002**, *1595*, 11 – 29.

(22) Panick, G.; Vidugiris, G. J. A.; Malessa, R.; Rapp, G.; Winter, R.; Royer, C. A. Exploring the Temperature Pressure Phase Diagram of Staphylococcal Nuclease. *Biochem.* **1999**, *38*, 4157–4164.

(23) Hummer, G.; Garde, S.; Garcia, A. E.; Paulaitis, M. E.; Pratt, L. R. The Pressure Dependence of Hydrophobic Interactions is Consistent with the Observed Pressure Denaturation of Proteins. *Proc. Natl. Acad. Sci.* **1998**, *95*, 1552–1555.

(24) Duan, Z.; Mao, S. A Thermodynamic Model for Calculating Methane Solubility, Density and Gas Phase Composition of Methane-bearing Aqueous Fluids from 273 to 523 K and from 1 to 2000 bar. *Geochim. Cosmochim. Act.* **2006**, *70*, 3369–3386.

(25) Sun, R.; Duan, Z. An Accurate Model to Predict the Thermodynamic Stability of Methane Hydrate and Methane Solubility in Marine Environments. *Chem. Geol.* **2007**, *244*, 248–262.

(26) Pruteanu, C. G.; Ackland, G. J.; Poon, W. C.; Loveday, J. S. When Immiscible Becomes Miscible—Methane in Water at High Pressures. *Sci. Adv.* **2017**, *3*, e1700240.

(27) Chandler, D. Interfaces and the Driving Force of Hydrophobic Assembly. *Nature* **2005**, *437*, 640.

(28) Strässle, T.; Saitta, A.; Le Godec, Y.; Hamel, G.; Klotz, S.; Loveday, J.; Nelmes, R. Structure of Dense Liquid Water by Neutron Scattering to 6.5 GPa and 670 K. *Phys. Rev. Lett.* **2006**, *96*, 067801.

(29) Grdadolnik, J.; Merzel, F.; Avbelj, F. Origin of Hydrophobicity and Enhanced Water Hydrogen Bond Strength near Purely Hydrophobic Solutes. *Proc. Natl. Acad. Sci.* **2017**, *114*, 322–327.

(30) Pruteanu, C. G.; Marenduzzo, D.; Loveday, J. S. Pressure-Induced Miscibility Increase of CH_4 in H_2O: A Computational Study Using Classical Potentials. *J. Phys. Chem. B* **2019**,

(31) Besson, J.; Nelmes, R. New Developments in Neutron-Scattering Methods under High Pressure with the Paris—Edinburgh Cells. *Phys. B: Cond. Matt.* **1995**, *213*, 31–36.

(32) Soper, A. Tests of the Empirical Potential Structure Refinement Method and a New Method of Application to Neutron Diffraction Data on Water. *Mol. Phys.* **2001**, *99*, 1503–1516.

(33) Li, M.; Li, F.; Gao, W.; Ma, C.; Huang, L.; Zhou, Q.; Cui, Q. Brillouin Scattering Study of Liquid Methane under High Pressures and High Temperatures. *J. Chem. Phys.* **2010**, *133*, 044503.

(34) Abramson, E. H.; Brown, J. M. Equation of State of Water based on Speeds of Sound Measured in the Diamond-Anvil Cell. *Geochim. Cosmochim. Act.* **2004**, *68*, 1827–1835.

(35) Kaminski, G.; Duffy, E. M.; Matsui, T.; Jorgensen, W. L. Free Energies of Hydration and Pure Liquid Properties of Hydrocarbons from the OPLS All-Atom Model. *J. Phys. Chem.* **1994**, *98*, 13077–13082.

(36) VandeVondele, J.; Krack, M.; Mohamed, F.; Parrinello, M.; Chassaing, T.; Hutter, J. Quickstep: Fast and Accurate Density Functional Calculations using a Mixed Gaussian and Plane Waves Approach. *Comp. Phys. Commun.* **2005**, *167*, 103–128.

(37) Becke, A. D. Density-Functional Exchange-Energy Approximation with Correct Asymptotic Behavior. *Phys. Rev. A* **1988**, *38*, 3098.

(38) Lee, C.; Yang, W.; Parr, R. G. Development of the Colle-Salvetti Correlation-Energy Formula into a Functional of the Electron Density. *Phys. Rev. B* **1988**, *37*, 785.

(39) Grimme, S.; Antony, J.; Ehrlich, S.; Krieg, H. A Consistent and Accurate Ab Initio Parametrization of Density Functional Dispersion Correction (DFT-D) for the 94 Elements H-Pu. *J. Chem. Phys.* **2010**, *132*, 154104.

(40) Krack, M. Pseudopotentials for H to Kr Optimized for Gradient-Corrected Exchange-Correlation Functionals. *Theor. Chem. Acc.* **2005**, *114*, 145–152.

(41) Bussi, G.; Donadio, D.; Parrinello, M. Canonical Sampling through Velocity Rescaling. *J. Chem. Phys.* **2007**, *126*, 014101.

(42) Hansen, P. H.; Rödner, S.; Bergström, L. Structural Characterization of Dense Colloidal Films Using a Modified Pair Distribution Function and Delaunay Triangulation. *Langmuir* **2001**, *17*, 4867–4875.

(43) Yarnell, J.; Katz, M.; Wenzel, R. G.; Koenig, S. Structure Factor and Radial Distribution Function for Liquid Argon at 85 K. *Phys. Rev. A* **1973**, *7*, 2130.

(44) Prescher, C.; Prakapenka, V. B.; Stefanski, J.; Jahn, S.; Skinner, L. B.; Wang, Y. Beyond Sixfold Coordinated Si in SiO_2 Glass at Ultrahigh Pressures. *Proc. Natl. Acad. Sci.* **2017**, *114*, 10041–10046.

(45) Koh, C. A.; Wisbey, R. P.; Wu, X.; Westacott, R. E.; Soper, A. K. Water Ordering around Methane during Hydrate Formation. *The Journal of Chemical Physics* **2000**, *113*, 6390–6397.

(46) Buchanan, P.; Aldiwan, N.; Soper, A.; Creek, J.; Koh, C. Decreased Structure on Dissolving Methane in Water. *Chemical physics letters* **2005**, *415*, 89–93.

(47) Sakamaki, R.; Sum, A. K.; Narumi, T.; Ohmura, R.; Yasuoka, K. Thermodynamic Properties of Methane/water Interface Predicted by Molecular Dynamics Simulations. *J. Chem. Phys.* **2011**, *134*, 144702.

(48) English, N. J.; Lauricella, M.; Meloni, S. Massively Parallel Molecular Dynamics Simulation of Formation of Clathrate-hydrate Precursors at Planar Water-methane Onterfaces: Insights into Heterogeneous Nucleation. *J. Chem. Phys.* **2014**, *140*, 204714.

(49) Sæthre, B. S.; van der Spoel, D.; Hoffmann, A. C. Free Energy of Separation of Structure II Clathrate Hydrate in Water and a Light Oil. *J. Phys. Chem. B* **2012**, *116*, 5933–5940.

(50) Jiang, H.; Jordan, K. D.; Taylor, C. E. Molecular Dynamics Simulations of Methane Hydrate Using Polarizable Force Fields. *J. Phys. Chem. B* **2007**, *111*, 6486–6492.

(51) Marzari, N.; Vanderbilt, D. Maximally Localized Generalized Wannier Functions for Composite Energy Bands. *Phys. Rev. B* **1997**, *56*, 12847.

(52) Santra, B.; Klimeš, J. c. v.; Alfè, D.; Tkatchenko, A.; Slater, B.; Michaelides, A.; Car, R.; Scheffler, M. Hydrogen Bonds and van der Waals Forces in Ice at Ambient and High Pressures. *Phys. Rev. Lett.* **2011**, *107*, 185701.

(53) Dion, M.; Rydberg, H.; Schröder, E.; Langreth, D. C.; Lundqvist, B. I. Van der Waals Density Functional for General Geometries. *Phys. Rev. Lett.* **2004**, *92*, 246401.

(54) Klimeš, J.; Bowler, D. R.; Michaelides, A. Chemical Accuracy for the Van der Waals Density Functional. *J. Phys.: Cond. Matt.* **2009**, *22*, 022201.

(55) Luzar, A.; Chandler, D. Hydrogen-bond Kinetics in Liquid Water. *Nature* **1996**, *379*, 55.

(56) Head-Gordon, T. Is Water Structure Around Hydrophobic Groups Clathrate-like? *Proc. Natl. Acad. Sci.* **1995**, *92*, 8308–8312.

(57) Santra, B.; Jr., R. A. D.; Martelli, F.; Car, R. Local Structure Analysis in Ab Initio Liquid Water. *Mol. Phys.* **2015**, *113*, 2829–2841.

(58) Ansari, N.; Dandekar, R.; Caravati, S.; Sosso, G.; Hassanali, A. High and Low Density Patches in Simulated Liquid Water. *J. Chem. Phys.* **2018**, *149*, 204507.

(59) Ansari, N.; Laio, A.; Hassanali, A. Spontaneously Forming Dendritic Voids in Liquid Water Can Host Small Polymers. *J. Phys. Chem. Lett.* **2019**, *10*, 5585–5591.

(60) Loveday, J.; Nelmes, R.; Guthrie, M.; Klug, D.; Tse, J. Transition from Cage Clathrate to Filled Ice: the Structure of Methane Hydrate III. *Phys. Rev. Lett.* **2001**, *87*, 215501.

(61) Ranieri, U.; Koza, M. M.; Kuhs, W. F.; Klotz, S.; Falenty, A.; Gillet, P.; Bove, L. E. Fast Methane Diffusion at the Interface of Two Clathrate Structures. *Nat. Commun.* **2017**, *8*, 1076.